Materials Horizons

Accepted Manuscript

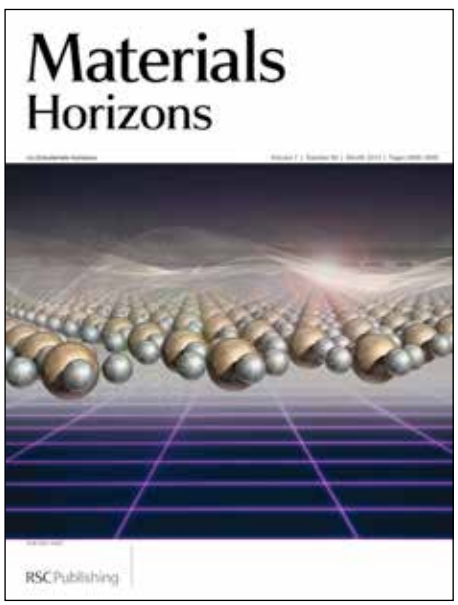

This is an *Accepted Manuscript*, which has been through the RSC Publishing peer review process and has been accepted for publication.

Accepted Manuscripts are published online shortly after acceptance, which is prior to technical editing, formatting and proof reading. This free service from RSC Publishing allows authors to make their results available to the community, in citable form, before publication of the edited article. This *Accepted Manuscript* will be replaced by the edited and formatted *Advance Article* as soon as this is available.

To cite this manuscript please use its permanent Digital Object Identifier (DOI®), which is identical for all formats of publication.

More information about *Accepted Manuscripts* can be found in the **Information for Authors**.

Please note that technical editing may introduce minor changes to the text and/or graphics contained in the manuscript submitted by the author(s) which may alter content, and that the standard **Terms & Conditions** and the **ethical guidelines** that apply to the journal are still applicable. In no event shall the RSC be held responsible for any errors or omissions in these *Accepted Manuscript* manuscripts or any consequences arising from the use of any information contained in them.

Cite this: DOI: 10.1039/c0xx00000x

www.rsc.org/xxxxxx

COMMUNICATION

Additive-assisted supramolecular manipulation of polymer:fullerene blend phase morphologies and its influence on photophysical processes

Ester Buchaca-Domingo,*[a] Andrew J. Ferguson,*[b] Fiona C. Jamieson,[c] Thomas McCarthy-Ward,[c] Safa Shoaee,[c] John R. Tumbleston,[d] Obadiah G. Reid,[b] Liyang Yu,[e] Marie-Beatrice Madec,[c,f] Martin Pfannmöller,[g] Felix Hermerschmidt,[a] Rasmus R. Schröder,[g,h] Scott Watkins,[i] Nikos Kopidakis,[b] Giuseppe Portale,[j] Aram Amassian,[e] Martin Heeney,[c] Harald Ade,[d] Garry Rumbles,[b,k] James R. Durrant[c] and Natalie Stingelin[a]

Received (in XXX, XXX) Xth XXXXXXXXX 20XX, Accepted Xth XXXXXXXXX 20XX
DOI: 10.1039/b000000x

It is well known that even small variations in the solid-state microstructure of polymer:fullerene bulk heterojunctions can drastically change their organic solar cell device performance. We employ pBTTT:$PC_{61}BM$ as a model system and manipulate co-crystal formation of 1:1 (by weight) blends with the assistance of fatty acid methyl esters as additives. This allows us to evaluate the role of the intermixed phase in such binary blends through manipulation of their phase morphology—from fully intercalated to partially and predominantly non-intercalated systems— and its effect on the exciton- and carrier- dynamics and the efficiency of charge collection, with relevance for future device design and manufacturing.

Despite the rapid and significant progress in polymer-fullerene blends for use as the light-harvesting active layer in Organic Photovoltaic (OPV) devices, there is still a lack of complete understanding of the actual phase morphology achieved in the active layer (*i.e.* the number of phases present and the consequent complexity of the resulting microstructure) and its correlation to device performance. Recently, significant efforts have been devoted to elucidate the role intermixed phases play. One of the best studied systems in this context is the bulk heterojunction (BHJ) composed of poly(3-hexylthiophene) (P3HT) and [6,6]-phenyl C_{61}-butyric acid methyl ester ($PC_{61}BM$), which has been investigated since the early 1990s,[1] and for which multiple phases have been identified. For instance, following the initial observation of polymer:fullerene miscibility and the measurement of a bimodal composition by Watts *et al.*, groups including Collins *et al.*, Treat *et al.* and Yin *et al.* found that PCBM aggregates and/or molecular species are miscible and mobile in disordered P3HT.[2] Pfannmöller *et al.* used Energy-filtered Transmission Electron Microscopy (EFTEM) to detect such a third intermixed ('composite') phase,[3] which exists in addition to the previously proposed BHJ microstructure of relatively phase-pure domains of the polymer and the fullerene. Further characterisation with X-ray diffraction and neutron reflectometry performed by Hyun Wook *et al.* showed that the mixing of P3HT and PCBM is influenced by many factors, such as the volumetric degree of ordering in the polymer and whether or not the PCBM is (pre-)aggregated.[4] Other authors have calculated the weight fraction of PCBM able to interdiffuse in regiorandom P3HT to be between 20 wt.% (for $PC_{61}BM$) to 41 wt.% (for $PC_{71}BM$).[5] It appears also that the high miscibility of fullerene derivatives with amorphous polymers or the disordered phase of semi-crystalline polymers is a rather universal behavior for binary polymer:fullerene systems;[6] however the ability to control the extent of mixing has not been demonstrated, and it is still poorly understood what the optimum phase morphology is for efficient devices.

Clearly, if we want to reach the maximum performance within polymer-fullerene BHJ solar cells, we need to gain a more in-depth knowledge and control of donor:acceptor blends in order to correlate their optical and electronic properties with their solid-state microstructure and phase morphology. Thereby, it is critical to identify the required fraction of intermixed phases that provides the best compromise between relevant optoelectronic processes for maximizing their photovoltaic performance. Here, we present a versatile way to manipulate, and thus easily study, such functional two-component, multi-phase blend architectures. We propose a strategy which exploits the fact that several conjugated polymers are capable of hosting certain fullerene derivatives such as $PC_{61}BM$ in "cavities" within their molecular arrangements to form what is termed a *co-crystal*,[7] representing an ordered intermixed phase in contrast to the intermixed amorphous solid-solutions formed by, for instance, the molecularly disordered fractions in P3HT:$PC_{61}BM$ binaries.

One example of such a co-crystal formation is the supramolecular arrangement obtained in blends of the thiophene-based polymer, poly(2,5-bis(3-alkyl-thiophene-2-yl)thieno[3,2-*b*]thiophene)s (pBTTT)[8-11] and $PC_{61}BM$, whose structure, photophysical properties and device performance have been well studied.[12-15] We have, for instance, previously shown that, films of this blend of 1:1 (by weight) composition comprise primarily the co-crystal, with minimal pure phases, resulting in rapid electron/hole recombination and consequently poor photocurrent generation, although there is still a measurable long-lived mobile polaron population.[16]

Co-crystal formation makes the binary pBTTT:$PC_{61}BM$ an ideal model system for controlling and characterizing the amount/type of phases that are present in this system by manipulation of the extent of fullerene intercalation in the polymer; *i.e.* by controlling the amount of this ordered intermixed phase. We therewith aim to answer the two following questions: (i) An intermixed phase (*i.e.* PCBM molecules intimately mixed with the polymer chains; in the present case-in-point, the co-crystal) seems to be present in many OPV devices: what is its importance and what role does it play in the photophysics? (ii) Can we design and fabricate an ideal phase morphology that maximizes the yield of long-lived free charges?

With these questions in mind we describe here a methodology to modify the phase morphology of 1:1 pBTTT:$PC_{61}BM$ blends using commercially available and economically viable additives. Through introduction of such additives, we induce either a fully intercalated, partially intercalated, or a predominantly non-intercalated system. We discuss how these changes in the phase morphology affect the exciton and carrier dynamics, and deduce the corresponding efficiency of charge collection.

We selected for our purpose *asymmetrical* compounds as processing aids—methyl esters of two fatty acids: dodecanoic acid methyl ester (Me12) and heptanoic acid methyl ester (Me7)—with the idea that their polar heads would favor $PC_{61}BM$ while their alkyl 'tail' would favor the side-chains of pBTTT. Figure 1a shows the chemical structures of pBTTT, $PC_{61}BM$ and these additives. We expected the additives to direct the supramolecular assembly of the two OPV components. Both additives, *i.e.* Me12 and Me7, were, however, not intended to act as plasticizers such as processing additives like 1,8-diiodooctane (DIO), 1,8-octanedithiol (ODT) and 1,8-dichlorooctane (DCO), which are symmetrical and frequently applied to modify the morphology of the active layer to realize an improvement of device performance.[17] Indeed, Cates *et al*. did not find improvement in device performance when using DIO in 1:1 pBTTT:$PC_{71}BM$ devices[14] indicating that these species cannot be used to control the phase morphology - which is the objective of this work.

When using 1:1 (by weight) pBTTT:$PC_{61}BM$ blends and adding 10 mol of the corresponding additive per monomer unit of the pBTTT, a first observation can be readily made: by varying the length of the alkyl 'tails' (C_7H_{15} vs. $C_{12}H_{25}$) of the additive the amount of fullerene that is intercalated in the polymer seems to be altered**.** Note here that thereby we found the use of additives with different tail lengths to be more efficient than varying the additive fraction. In fact, the longer alkyl additive seems to be able to expel considerable fractions of the fullerene, leading to a noticeable amount of relatively phase-pure pBTTT regions. This can be deduced from the Grazing-Angle Incidence Wide-Angle X-ray Scattering (GIWAXS) data shown in Figure 1b, where we compare the neat polymer (*i*), with the pBTTT:$PC_{61}BM$ binary (*ii*) and the corresponding ternary systems. In the pBTTT:$PC_{61}BM$ blend (*ii*), the first (100) polymer diffraction order at $q \sim 0.28$ Å^{-1} is shifted to higher distances ($q \sim 0.2$ Å^{-1}) due to co-crystal formation.[11-14] However, when Me12 (*iii*) and Me7 (*iv*) are introduced into the system, we observe two (100) diffractions, one at $q \sim 0.2$ Å^{-1} characteristic for the co-crystal, and one at $q \sim 0.28$ Å^{-1} that can be attributed to the neat polymer. This is a clear indication that for both ternaries the formation of an intercalated phase is at least partly prevented, with the Me12 additive seeming to have a more pronounced effect, leading to a higher fraction of phase-pure pBTTT domains, as evident from the stronger diffraction observed at $q \sim 0.28$ Å^{-1} for this ternary compared to the system comprising Me7.

These findings are supported and quantified by Scanning Transmission X-ray microscopy (STXM; Figure 1c/d), which also allows us to determine the composition of the different blends. Figure 1d displays absorbance measurements near the carbon 1s absorption edge of pBTTT:$PC_{61}BM$ blend films (along the white lines indicated in the different panels of Figure 1c), processed with Me12 (*iii*) and Me7 (*iv*) and without additives (*ii*). The spectra are fit using a linear combination of the neat pBTTT and $PC_{61}BM$ reference spectra following previously established procedures.[5,6c,18] We find that both the pBTTT:$PC_{61}BM$ binary (*ii*) and the pBTTT:Me7:$PC_{61}BM$ ternary (*iv*) comprise a similar average PCBM content in the pBTTT matrix: about 42 wt. % and 43 wt.%, respectively. These data reinforce the idea that a considerable fraction of intermixed phase is still present in the blends comprising the short-chain additive Me7 (*iv*), as also indicated by the pronounced diffraction at $q \sim 0.2$ Å^{-1} in GIWAXS. In contrast, only about 19 wt.% of $PC_{61}BM$ is detected in blends comprising Me12 (*iii*), supporting the picture that longer additives such as Me12 are able to efficiently macro-phase separate the polymer and the fullerene and, thus, deplete a larger amount of $PC_{61}BM$ molecules from the mixed phase (here, the co-crystal), leading to a phase morphology dominated by the co-existence of relatively pure phases of both components (*i.e.* pBTTT and $PC_{61}BM$).

Optical microscopy highlights the consequence the various phase morphologies has on the film-forming characteristics of these blends (see Supplementary Figure S1/a): the presence of additives increases the surface roughness of the films, which exhibit large fullerene domains (verified with STXM) when the long-chain additive Me12 is used, likely due to the phase separation of the polymer and fullerene, leading to a stronger aggregation of the $PC_{61}BM$ component in pBTTT:Me12:$PC_{61}BM$ ternaries. In addition, we found that longer tailed additives, such as $C_{13}H_{27}$ (called here Me14), are able to expel even higher amounts of $PC_{61}BM$ as shown in Supplementary Figure S1a/b. Note that the features observed in pBTTT:Me7:$PC_{61}BM$ microscope images are due to surface roughness and not large-scale phase separation. This was confirmed with STXM data at different photon energies supporting that those features seen for pBTTT:Me7:$PC_{61}BM$ are not $PC_{61}BM$ aggregates (see Supplementary Figure S1/c). At the same time, Resonant Soft X-ray scattering (R-SoXS)[19] shows that films comprising Me12 and Me7 have nano-morphologies with very similar spatial frequency distributions that are characterized by a median characteristic length scale of ~ 25 nm (see Supplementary Figure S2). Moreover RSoXS data show different intensities for *ii* and *iv* providing further evidence that pBTTT:Me7:$PC_{61}BM$ consists of a 3-phase morphology producing contrast between the co-crystal (*i.e.* fully intercalated) phase as well as the (relatively) phase-pure

polymer and $PC_{61}BM$ regions. In contrast, the pBTTT:$PC_{61}BM$ binary forms a 1-phase system quenching any possible contrast between the polymer and the fullerene over the measurement length scale of R-SoXS (10 nm to 1 µm). Note also that the separation between polymer chains for the fully intercalated blend is ~ 3nm (from WAXS measurements), which is below the smallest lengths scale probed with R-SoXS. Thus, only volume fraction and not the length scale of the nano-morphology was manipulated.

The latter observation is in agreement with data obtained by Time-correlated Single-photon Counting (TCSPC), where the photoluminescence (PL) decays (Figure 2a) are close to the instrument response limit for both the pBTTT:$PC_{61}BM$ binary (*ii*) and pBTTT:Me7:$PC_{61}BM$ ternary (*iv*), *i.e.* systems for which GIWAXS indicates the presence of a considerable amount of intercalated material. Apparently, the fine intermixing of the donor and acceptor molecules, as found in a co-crystal, results in very rapid exciton quenching.[16b] In contrast, the PL decay measured for pBTTT:Me12:$PC_{61}BM$ (*iii*), whilst still strongly quenched relative to neat pBTTT [note we show here the decay of pBTTT:Me12 (*v*) which is similar to the neat polymer], is significantly slower than those observed for the pBTTT:$PC_{61}BM$ (*ii*) and pBTTT:Me7:$PC_{61}BM$ (iv) blends, pointing to the fact that excitons are longer-lived in these samples. Since ternaries comprising Me12 (*iii*) appear to possess a microstructure comprising more defined, relatively phase-pure pBTTT as indicated by our GIWAXS and STXM data, the extended exciton lifetime is likely to result from the necessity for the exciton to reach an interface between the neat pBTTT and $PC_{61}BM$ domains. Note though that the steady-state photoluminescence quenching (PLQ) for all systems comprising $PC_{61}BM$ was high (Figure 2b); the addition of fatty acid methyl esters did decrease the PLQ, with the pBTTT:Me12:$PC_{61}BM$ ternaries featuring the least quenching in agreement that Me12 is better able to prevent intercalation of the fullerene into the pBTTT than its Me7 counterpart.

Based on the GIWAXS, STXM, R-SoXS, TCSPC and PLQ data we conclude that the microstructure of pBTTT:$PC_{61}BM$ systems can be manipulated by use of additives and they can be utilized to control the amount/type of phases present depending on their precise nature (see schematics presented in Figure 2c). The pBTTT:$PC_{61}BM$ binary (*ii*), at the composition selected (1:1 by weight) is well known to form a co-crystal (*i.e.* a 1-phase system) in agreement with our data. When adding Me12 to the system, a considerable amount of the fullerene is expelled into macrophase-separated domains, lowering the average PCBM concentration of the nano-morphology. Hence, a noticeable fraction of neat pBTTT and, likely, neat $PC_{61}BM$ phases are present in these thin-film architectures, with the phase separation being directed by the Me12 (*iii*). Me7 seems less efficient to induce phase separation; as a consequence a 3-phase morphology is induced in pBTTT:Me7:$PC_{61}BM$ ternaries (*iv*) that is dominated by the highly intermixed phase comprising the co-crystal, with the pure pBTTT and $PC_{61}BM$ regions being minority phases.

Having established a microstructural picture of the various binaries and ternaries discussed here, we probed their electronic landscape, and in particular, the photoinduced charge carrier generation and decay in such systems. To this end, we performed Transient Absorption Spectroscopy (TAS) and Time-Resolved Microwave Conductivity (TRMC) measurements. TRMC is a contactless, pump-probe technique that is sensitive to mobile carriers and is a complementary technique to TAS. Charge generation and decay are monitored through the time-resolved changes in absorbed microwave power by the sample, which are related to the transient photoconductance, $\Delta G(t)$.[20] Note though that with both techniques also relevant information on the phase morphology can be deduced; for instance, Jamieson *et al.* recently reported TAS data of pBTTT:$PC_{61}BM$ blends of varying composition, where significant generation of long-lived charges was only observed for $PC_{61}BM$ loadings ≥50 wt. %,[16a] corresponding to a composition where all available intercalation sites are filled and relatively phase-pure $PC_{61}BM$ domains are formed; while with TRMC, Rance et *al.* showed for pBTTT:fullerene blends, that upon formation of pure domains of $PC_{71}BM$ or bis-$PC_{61}BM$ mobile electrons also begin to contribute to the high-frequency mobility and enhanced mobile carrier lifetimes are observed.[16b]

We first discuss the TAS data obtained on the various pBTTT:$PC_{61}BM$ blends, measured by monitoring the absorbance of pBTTT polarons at 980 nm (Figure 3a). The observed transients all exhibit similar power-law decays on the 20 – 400 ns timescale, characteristic of non-geminate recombination of separated (free) polarons.[21] The magnitude of these signals is therefore indicative of the yields of dissociated polarons. The largest photoinduced absorption (ΔOD) is observed for the pBTTT:Me7:$PC_{61}BM$ (*iv*) ternary, indicating that this 3-phase system which comprises a considerable amount of intermixed phase in the form of the co-crystal beside some predominantly pure regions of pBTTT and possibly $PC_{61}BM$, exhibits the highest separated polaron yield (Table 1).

A similar trend is observed in the corresponding photoconductance transients obtained in TRMC (Figure 3b). The decay dynamics are, for instance, comparable to those observed in TAS, indicating that they are indeed dominated by non-geminate recombination, as discussed above. Also, the highest photoconductance signal is again obtained for the pBTTT:Me7:$PC_{61}BM$ system (*iv*), followed by the pBTTT:Me12:$PC_{61}BM$ ternary (*iii*). The lowest signal is observed for the pBTTT:$PC_{61}BM$ binary (*ii*). [Note that the photoconductance of pBTTT:Me12 (*v*) is also plotted here to demonstrate that these additives do not change significantly the mobilities of holes inside neat pBTTT. An essentially identical behavior was observed for pBTTT:Me7].

We furthermore estimated the charge-carrier yield combining our TRMC data with those obtained from TAS and photoluminescence decay measurements (Table 1). For this purpose we utilized the fact that the measured peak photoconductance signal is related to the product of the yield for free carrier generation and the sum of the mobilities of free charge carriers ($\phi\Sigma\mu$), as shown in Equation 2 in the Experimental Section. By extrapolating the peak photoconductance signal to the linear regime at low light intensities (see Supporting Information Figure S3), using

Equation 3 in the Experimental Section, we can estimate the peak $\phi\Sigma\mu$ values for neat pBTTT, and all blends with and without additives. For the neat pBTTT (as well as binaries of the polymer with the additives, *i.e.* pBTTT:Me7 and pBTTT:Me12), we moreover assume that photoinduced electrons are trapped and that the photoconductance is therefore dominated by mobile holes, which possess a high-frequency mobility of ~0.01 cm^2/Vs.[22] This results in a free-carrier yield in the neat polymer of ~2.5% which increases slightly (but remains very low) for pBTTT:Me7 (2.7%) and pBTTT:Me12 (2.9%).

The situation changes when $PC_{61}BM$ is added to the polymer or polymer:additive system: for all blend films studied photoluminescence quenching data (steady-state and time-resolved) indicates that the efficiency of PBTTT exciton quenching is ≥ 75%. As such, the increase in separated polaron yields observed in the TRMC and TAS data with methyl ester addition cannot be assigned to enhanced exciton quenching with respect to the pBTTT:$PC_{61}BM$ binary (indeed Me12 addition slightly reduces the efficiency of exciton quenching). We have previously reported that the long-lived polaron yields observed for the 1:1 (by weight) pBTTT:$PC_{61}BM$ binary in the absence of additives is partially limited by electron/hole recombination in the highly intermixed co-crystal in the film.[16a] As such the increase in the long-lived separated polaron yields with methyl ester addition can be assigned to increased phase segregation, as indicated from the structural data above, with the presence of relatively pure pBTTT and $PC_{61}BM$ phases assisting the co-crystal in spatial separation of photogenerated electrons and holes.

In the following we attempt to quantify the separated polaron yields and determine the contribution of mobile electrons to the measured photoconductance signals for the blends with $PC_{61}BM$ (Table 1). For the pBTTT:$PC_{61}BM$ binary, which is fully intercalated, we assume that the electrons are unable to resonate at the frequency of the microwave probe beam, consistent with the observations made for blends of pBTTT with $PC_{71}BM$, another fullerene derivative, prior to the formation of relatively phase-pure acceptor domains at higher $PC_{71}BM$ loadings.[16b] This results in a predicted free-carrier yield of ~33%, indicating that intimate mixing of the polymer and fullerene derivative in this blend results in reasonably efficient dissociation of excitons into long-lived free carriers. However, the relative exciton lifetimes in neat pBTTT and pBTTT:$PC_{61}BM$, as measured using TCSPC, indicate an exciton quenching yield of ~95% in the blend. The discrepancy between the yields predicted from the PL lifetimes and the photoconductance signal observation suggests that there is an additional process that results in exciton quenching but does not give rise to mobile carriers, presumably due to rapid electron/hole recombination below the response time of our TRMC system. [We note that in previous work the binary pBTTT:fullerene films were subjected to a high temperature anneal at 180 °C that drives extensive formation of the fully intercalated co-crystal and leads to higher yield for free carrier generation measured by TRMC than obtained here.[16b] The high temperature anneal is not performed here since the scope of our study is to control the morphology by using appropriate additives.]

For the pBTTT:Me7:$PC_{61}BM$ blends, we use the exciton lifetime measured by TCSPC to estimate the maximum possible free carrier yield, also giving a value of 95%. Since the data for the pBTTT:$PC_{61}BM$ binary suggests that intercalation results in a large discrepancy between the exciton quenching and free carrier yield, this value of 95% represents an upper limit for the free carrier yield in pBTTT:Me7:$PC_{61}BM$; which means that the lower limit for the mobility sum, $\Sigma\mu$, is ~0.027 cm^2/Vs. This calculation implies that mobile electrons begin to contribute to the measured photoconductance signal in pBTTT:Me7:$PC_{61}BM$ ternaries (contrary to pBTTT:$PC_{61}BM$ systems), likely because some phase-pure $PC_{61}BM$ domains are formed as a result of the expulsion of the fullerene from the pBTTT domains by the Me7 additive (as observed in GIWAXS), confirming our picture of a three-phase morphology in this ternary system.

For pBTTT:Me12:$PC_{61}BM$ samples, we can also use our TCSPC data in combination with the relative transient polaron absorption to estimate upper and lower limits for the free carrier yield. This approach results in values for ϕ of 36 and 75%, which places bounds on $\Sigma\mu$ of 0.015 and 0.031 cm^2/Vs. The presence of a reduced amount of intimately mixed pBTTT and $PC_{61}BM$ in this ternary suggests that once again the free carrier yield is likely to tend toward to lower value, which suggests that mobile electrons can also be detected for this ternary, consistent with our structural analysis, which indicates the presence of considerable fractions of relatively phase-pure $PC_{61}BM$ domains.

The question that remains is how these changes in exciton and charge-carrier generation and dynamics affects device performance. To this end, we fabricated OPV devices coating the active layer with a wire-bar coater, the performance of which was highly reproducible (see Figure 4a and Supplementary Table S1). For the pBTTT:$PC_{61}BM$ binary (*ii*) we observe poor OPV performance, with low open-circuit voltage (V_{oc}), short-circuit current (J_{sc}), and fill factor (*FF*), consistent with previous reports[12-14] and in agreement with extensive $PC_{61}BM$ intercalation and the absence of neat domains of the fullerene derivative, which results in rapid electron/hole recombination preventing extraction of charges from the device and thus low photocurrent density.[14,16a] Devices fabricated using the pBTTT:Me12:$PC_{61}BM$ ternary (*iii*) as the active layer show a slight improvement in device performance, mainly due to improved J_{sc} and *FF*. In accord with the TAS and TRMC data, the optimum performance is achieved for pBTTT:Me7:$PC_{61}BM$ (*iv*) active layer. Our data, hence, support the picture that an optimum phase morphology is present in systems where charge generation occurs in a finely intermixed polymer/fullerene phase followed by spatial separation of electrons and holes at the interface of this mixed phase and relatively phase-pure domains of the polymer or the fullerene.[16a] The presence of a relatively large fraction of such an intermixed phase coexisting with pure domains appears favorable. Indeed, the ternaries comprising the Me12 additive, leading to a more pronounced phase-segregation of the pBTTT and $PC_{61}BM$, seem to be somewhat limited by exciton diffusion. Moreover, our work shows that quite a considerable amount of intermixed phase needs to be present for efficient device performance. So far common believe in the field has generally been that large amounts of phase-pure domains will lead to optimum OPV efficiency. It is also rather unambiguous from our data that fully intermixed systems are detrimental for OPV device performance: the binary pBTTT:$PC_{61}BM$ blend, as well as the

ternary pBTTT:Me7:$PC_{61}BM$ blend (*iv*) after annealing at 150 °C (^{ann}*iv*)—leading also to a fully intercalated blend [see Electron Spectroscopic Images (ESI) in Figure 4b and temperature-dependent WAXS data in the Supplementary Information S4]—feature the lowest device efficiencies.

Finally, we note that Bartelt *et al*. have recently come to very similar conclusions having investigated a three-phase morphology that included an amorphous, mixed regions, the composition of which was manipulated by annealing.[6a] The presence of the mixed region was critical and required a specific threshold PCBM concentration to be reached for high performance. Intercalation, as used here, is a natural way of keeping the PCBM concentration in the mixed regions sufficiently high.

Conclusions

We demonstrated that the extent of intercalation of $PC_{61}BM$ into the crystalline domains of pBTTT can be controlled through the use of long fatty acid methyl ester as additives. We showed that the shorter chain additive, Me7, hinders to a certain extent intercalation of $PC_{61}BM$ into the polymer structure, resulting in the formation of a 3-phase system, consisting of predominantly intercalated co-crystals that co-exist with relatively pure pBTTT and $PC_{61}BM$ minority phases. [Note: we do not exclude the presence of partially intercalated co-crystals]. In contrast, the longer chain additive, Me12, appears to be more effective in preventing formation of co-crystalline structures and leads to a more pronounced macro-phase separation of pBTTT and $PC_{61}BM$. We used TAS and TRMC spectroscopic techniques to show that in the presence of $PC_{61}BM$, exciton quenching and free carrier generation are enhanced in all blends. In the absence of any additives, *i.e.* in the case of the fully-intercalated 1:1 pBTTT:$PC_{61}BM$ binary, the efficient exciton quenching does, however, not correlate with quantitative free carrier formation. An optimum free carrier yield is obtained for the partially-intercalated pBTTT:Me7:$PC_{61}BM$ ternary comprising a considerable fraction of co-crystal, which seems to also provide the ideal microstructure for long-range carrier transport. Our results highlight the importance of having a certain amount of relatively pure domains of either the polymer or the fullerene or both.[23] These can act as energetic sinks for the generation of charges, relative to amorphous or mixed domains,[16a] and/or provide an entropic (carrier density gradient) driving force due to formation of the carriers in the mixed phase and lack of electron density in the relatively phase-pure $PC_{61}BM$ phase.[16b] In the strongly phase-separated pBTTT:Me12:$PC_{61}BM$ blend, free carrier formation seems to be limited by the ability of the pBTTT excitons to reach the interface with $PC_{61}BM$, resulting in a reduced OPV device performance, despite the presence of some neat $PC_{61}BM$ domains capable of transporting electrons. Reassuringly, the spectroscopic data are consistent with the microstructures predicted by structural techniques and schematically drawn in Figure 2c. For instance, the three-phase morphology achieved with the Me7 additive will enhance charge formation due to a large donor-acceptor interface within the co-crystal (the intermixed phase), while also providing a network of neat $PC_{61}BM$ to maximize the long-lived carrier density and facilitate carrier extraction in a device.

In summary, we, for the first time, provide donor:acceptor blends that are structurally well-defined whereby we can manipulate the intermixed phases present and, thus, the phase morphology of such systems. Hence, our work is contributing to the on-going discussion stimulated by, for instance, Treat *et al.* and Collins *et al.*[2b,c] and will assist in establishing guidelines to fabricate high-performance reproducible devices by selecting the individual components for their both electronic properties as well their structural compatibility. Despite these observations that the microstructure can be easily controlled by use of suitable additives a number of questions remain: (i) How much of this intermixed phase is actually present for the ternary system with Me7? (ii) What are the dimensions of the formed domains? (iii) How does the phase morphology affect the energy levels of the individual phases? (iv) How does the microstructure affect the photocarrier dynamics and carrier transport; and (v) which is the mechanism behind these additives? These are questions that we are intending to address in future.

Experimental section

pBTTT was synthesized as reported previously ($M_w \approx 66$ kg/mol, $M_n \approx 34$ kg/mol) and measured by GPC against polystyrene standards.[24] $PC_{61}BM$ was purchased from Solenne and used as received. Heptanoic acid methyl ester (Me7) and dodecanoic acid methyl ester (Me12) additives were purchased from Fluka and Aldrich, respectively. Solutions were prepared weighing a 1:1 (by mass) mixture of pBTTT and $PC_{61}BM$, and then adding 10 mol of the respective additive per monomer unit of the polymer (11 µL of Me7 and 16.4 µL of Me12). The total concentration of the pBTTT:PCBM mixture was 20 mg/mL in 1,2-ortho-dichlorobenzene (1,2-oDCB, Aldrich) and all solutions were left stirring for more than 4 hours at 100 °C to fully dissolve the active material. *Grazing-Angle Incidence Wide-Angle X-ray Scattering (GIWAXS)* measurements were carried out at D-line at the Cornell High Energy Synchrotron Source (CHESS) at Cornell University. A 0.5 × 0.1 mm beam size with a wavelength of 1.15 Å and wide band pass (1.47%) was generated from double-bounce multilayer monochromator. The incidence angle was 0.15° with respect to the substrate plane, as established by performing X-ray reflectivity using an ion chamber. A 50 × 50 mm charged coupling device (CCD) area detector (Medoptics) with pixel size of 46.9 µm was placed at a distance of 103.6 mm from the sample stage. A 1.5 mm-wide tantalum rod was used to block the intense scattering at low angles of incidence. Films were deposited on glass by wire-bar coating from hot solution (~85-90 °C) at RT or 35 °C. *Variable temperature WAXS* measurement was performed at BM26B-DUBBLE Dutch-Belgian beamline of the European Synchrotron Radiation Facility (ESRF) equipped with a Linkam THMS600 temperature-controlled stage. Film was prepared by drop-casting a hot 1,2-oDCB solution onto substrate kept at RT. The obtained film was powdered and then placed between Kapton sheets properly pressed. *Scanning Transmission X-ray Microscopy (STXM) and Resonant Soft X-ray scattering (R-SoXS)* were conducted at Beamline 5.3.2.2[25] and 11.01.2[19b], of the Advanced Light Source at Lawrence Berkeley National Laboratory, respectively. For these measurements, films were deposited onto polystyrene sulfonate (PSS)-coated glass substrates by wire-bar coating hot

solutions (~85-90 °C) at RT or 35 °C and then floated onto TEM grids. *Photoluminescence decays* were recorded, for films prepared by drop-casting hot 1,2-oDCB solutions onto substrates kept at either RT or 35 °C, after excitation at 550 nm with a 10 MHz train of pulses (Pulse-width: ~6 ps fwhm; Instrument Response Function: ~160 ps fwhm) from a high-power fiber laser (Fianium WhiteLase Supercontinuum SC400-2), for emission at 725 nm, with a cooled photon counting photomultiplier tube (Hamamatsu H6279), using the time-correlated single-photon counting technique.[26] The PL decays were analyzed using an established non-linear least squares iterative reconvolution procedure,[27] where the finite width of the instrument response function was effectively deconvoluted from the measured data to give an overall temporal response of ~20 ps. Data were fit to a sum of two or three exponentials and the quality of fit judged using stringent statistical procedures. [26] *Photoluminiscence quenching* was measured using steady state spectrofluorimeter (Horiba Jobin Yvon, Spex FLuoromax 1), all films were deposited on glass by wire-bar coating from hot solution (~85-90 °C) at RT or 35 °C and excited at their absorption maxima. *Transient absorption (TA) decays* were measured by exciting the sample film, under a nitrogen (and oxygen) atmosphere, pumped with a Nd:YAG laser (Lambda Photometrics). The excitation wavelength used was 560 nm, with a pump intensity of 0.4 - 50 μJcm^{-2} and a repetition frequency of 20 Hz. A photodiode (Thorlabs ITC502) was used as the probe. The probe light passing through the sample film was detected with a silicon photodiode (Hamamatsu Photonics, S1722-01). The signal from the photodiode was pre-amplified and sent to the main amplification system (Costronics Electronics). The amplified signal was collected with a digital oscilloscope (Tektronics, TDS220), which was synchronised with a trigger signal of the pump laser pulse from a photodiode (Thorlabs Inc., DET210). To reduce stray light, scattered light and sample emission, appropriate optical cut-off filters were placed before and after the sample. Films were deposited on glass by wire-bar coating from hot solution (~85-90 °C) at RT or 35 °C. *Time-Resolved Microwave Photoconductivity*. Films were prepared by drop-casting hot 1,2-oDCB solutions onto substrates kept at either RT or 35 °C. Photocarrier dynamics were studied using time-resolved microwave photoconductivity (TRMC), a contactless, pump-probe technique where both the initial generation of mobile carriers and their eventual decay back to equilibrium are monitored through the time-resolved changes in absorbed microwave power by the sample.[20a,28] TRMC measurements were performed at NREL using a system that has been described fully elsewhere.[28b,29] The sample was placed in an X-band microwave cavity terminated with a grating reflective to microwaves but transparent to the optical excitation that was used to generate carriers within the film. All drop cast films were excited with 5 ns laser pulses at 550 nm from an optical parametric oscillator (Continuum Panther) pumped by a Q-switched Nd:YAG laser (Continuum Powerlite). The transient change in photoconductance, $\Delta G(t)$, was measured via changes in the microwave power, $\Delta P(t)$, due to absorption of microwaves by the generated carriers, and is given by:

$$\Delta G(t) = -\frac{1}{K}\frac{\Delta P(t)}{P} \quad (1)$$

where K is a calibration factor experimentally determined from the resonance characteristics of the microwave cavity and the dielectric properties of the sample.[28b,29-30] The peak photoconductance, ΔG_{EOP}, probed by TRMC includes the density of free carriers multiplied by their mobility:

$$\Delta G_{EOP} = \beta q_e I_0 F_A \phi \Sigma\mu \quad (2)$$

where β relates to the dimension of the waveguide cross-section, q_e is the elementary electronic charge, I_0 is the incident photon fluence, F_A is the fraction of absorbed photons, ϕ is the yield for free carrier generation, and $\Sigma\mu$ is the sum of free carrier mobilities. It should be noted here that the mobility probed by TRMC is the local mobility of free carriers (electrons and holes) probed by their absorption of the 9 GHz microwave beam. This high-frequency mobility is not necessarily directly related to the mobility determined in bulk (device-type) measurements, where the carrier has to traverse the entire device and the extracted bulk mobilities are typically limited by features such as grain boundaries.

The sub-linear dependence of the peak photoconductance, ΔG_{EOP}, can be extrapolated to the linear response limit using:

$$\frac{\Delta G_{EOP}}{\beta q_e} = \frac{A I_0 F_A}{1 + \sqrt{B I_0 F_A}} \quad (3)$$

where A and B are fitting parameters. Comparison of equations 2 and 3 allows us to obtain the low-intensity, linear response limit as $A = [\phi\Sigma\mu]$. *Solar cell devices* were made by first spin-coating a layer of PEDOT:PSS (50 nm, clevios AI4083) onto the ITO coated glass substrate and annealing in air at 150 °C. The active layer was then deposited by wire-bar coating hot solutions (~85-90 °C) at RT or 35 °C. The samples were then transferred to a glovebox where cathode made of calcium (20 nm thick) and aluminium (100 nm thick) were deposited by evaporation under a vacuum of less than 10^{-6} mbar using a shadow mask to define pixels of 0.15 cm^2 and 1 cm^2. *Electron Spectroscopic Imaging (ESI)* measurements were performed with a Libra 200 Cs MC from Carl Zeiss Microscopy GmbH and a Camera TemCam-F416 with Software EM-MENU (TVIPS GmbH). Films were deposited onto polystyrene sulfonate (PSS)-coated glass substrates by wire-bar coating hot solutions (~85-90 °C) at RT or 35 °C and then floated onto TEM grids; images were obtained as described previously.[3]

Acknowledgements

The authors are very grateful to Lee J. Richter and Dean M. DeLongchamp and Paul Smith for highly fruitful and stimulating discussions regarding this manuscript, as well as Richard Sweeney and Pabitra Shakya Tuladhar for their help. This work was supported by UK's Engineering and Physical Sciences Research Council (EP/J500021/1 and EP/G060738/1) and a KAUST Global Collaborative Research Academic Excellence Alliance (AEA) grant. NS is in addition supported by a European Research Council (ERC) Starting Independent Research Fellowship under the grant agreement No. 279587. The TRMC system described here was funded by the Solar Photochemistry Program, Division of Chemical Sciences, Geosciences, and Biosciences, Office of Basic Energy Sciences, U.S. Department

of Energy (DOE), Grant DE-AC36-08GO28308. The experimental implementation of the TRMC technique was supported by the Laboratory Directed Research and Development (LDRD) Program at the National Renewable Energy Laboratory under task number 06RF1201. STXM and R-SoXS characterization and analysis by JT and HA were supported by Materials Chemistry Program, Materials Sciences and Engineering Division, Office of Basic Energy Sciences, DOE, Grant DE-FG02-98ER45737; data were acquired at Beamline 5.3.2.2[25] and 11.01.2[19b] of the ALS, which is supported by DOE (DE-AC02-05CH1123). Thanks is also given to David Kilcoyne for instrument support. Finally, the authors extend their thanks to ESRF (Dubble Beamline) for their assistance with the temperature-dependent WAXS experiment.

Notes and references

[a] *Department of Materials and Centre for Plastic Electronics, Imperial College London, London, UK; E-mail: e.buchaca-domingo@imperial.ac.uk*
[b] *Chemical and Materials Science Center, National Renewable Energy Laboratory, Golden, Colorado, USA; E-mail: andrew.ferguson@nrel.gov*
[c] *Department of Chemistry and Centre for Plastic Electronics, Imperial College London, London, UK*
[d] *Department of Physics, North Carolina State University, Raleigh, North Carolina, USA*
[e] *Division of Physical Sciences and Engineering, King Abdullah University of Science and Technology (KAUST), Thuwal, Saudi Arabia*
[f] *Solvay Interox, Warrington, UK*
[g] *CellNetworks, BioQuant, Heidelberg University, Heidelberg, Germany*
[h] *InnovationLab GmbH, Heidelberg, Germany*
[i] *Commonwealth Scientific and Industrial Research Organisation, Clayton, Australia*
[j] *ESRF Grenoble, Grenoble, France*
[k] *Department of Chemistry and Biochemistry, University of Colorado, Boulder, USA*

1 (a) J. F. Chang, J. Clark, N. Zhao, H. Sirringhaus, D. W. Breiby, J. W. Andreasen, M. M. Nielsen, M. Giles, M. Heeney, I. McCulloch, *Phys Rev. B,* 2006, **74**, 115318; (b) R. Zhang, B. Li, M. C. Iovu, M. Jeffries-El, G. Sauvé, J. Cooper, S. Jia, S. Tristram-Nagle, D. M. Smilgies, D. N. Lambeth, R. D. McCullough, T. Kowalewski, *J. Am. Chem. Soc.*, 2006, **128**, 3480; (c) M. Theander, O. Inganäs, W. Mammo, T. Olinga, M. Svensson, M. R. Andersson, *J. Phy. Chem. B*, 1999, **103**, 7771; (d) K. E. Aasmundtveit, E. J. Samuelsen, W. Mammo, M. Svensson, M. R. Andersson, L. A. A. Pettersson, O. Inganäs, *Macromolecules*, 2000, **33**, 5481; (e) I. F. Perepichka, D. F. Perepichka, H. Meng, F. Wudl, *Adv. Mater.*, 2005, **17**, 2281.

2 (a) B. Watts, W. J. Belcher, L. Thomsen, H. Ade, P. C. Dastoor, *Macromolecules* 2009, **42**, 8392; (b) B. A. Collins, E. Gann, L. Guignard, X. He, C. R. McNeill, H. Ade, *J. Phys. Chem. Lett.*, 2010, **1**, 3160; (c) N. D. Treat, M. A. Brady, G. Smith, M. F. Toney, E. J. Kramer, C. J. Hawker, M. L. Chabinyc, *Adv. Energy Mater.*, 2011, **1**, 1; (d)W. Yin, M. Dadmun, *ACS Nano*, 2011, **5**, 4756.

3 M. Pfannmo□ller, H. Flu□gge, G. Benner, I. Wacker, C. Sommer, M. Hanselmann, S. Schmale, H. Schmidt, F. A. Hamprecht, T. Rabe, W. Kowalsky, R. R. Schro□der, *Nano Lett.*, 2011, **11**, 3099.

4 H. W. Ro, B. Akgun, B. T. O'Connor, M. Hammond, R. J. Kline, C. R. Snyder, S. K. Satija, A. L. Ayzner, M. F. Toney, C. L. Soles, D. M. DeLongchamp, *Macromolecules*, 2012, **45**, 6587.

5 X. He, B. A. Collins, B. Watts, H. Ade, C. R. McNeill, *Small*, 2012, **8**, 1920.

6 (a) J. A. Bartelt, Z. M. Beiley, E. T. Hoke, W. R. Mateker, J. D. Douglas, B. A. Collins, J. R. Tumbleston, K. R. Graham, A. Amassian, H. Ade, J. M. J. Fréchet, M. F. Toney, M. D. McGehee, *Adv. Energy Mater.*, 2013, **3**, 364; (b) J. R. Tumbleston, A. C. Stuart, E. Gann, W. You, H. Ade, *Adv. Funct. Mater.*, 2013, **23**, 3463; (c) B. A. Collins, Z. Li, J. R. Tumbleston, E. Gann, C. R. McNeill, H. Ade, *Adv. Energy Mater.*, 2013, **3**, 65; (d) B. A. Collins, Z. Li, C. R. McNeill, H. Ade, *Macromolecules*, 2011, **44**, 9747; (e) N. D. Treat, A. Varotto, C. J. Takacs, N. Batara, M. Al-Hashimi, M. J. Heeney, A. J. Heeger, F. Wudl, C. J. Hawker, M. L. Chabinyc, *J. Am. Chem. Soc.*, 2012, **134**, 15869.

7 N. C. Miller, E. Cho, R. Gysel, C. Risko, V. Coropceanu, C. E. Miller, S. Sweetnam, A. Sellinger, M. Heeney, I. McCulloch, J. L. Brédas, M. F. Toney, M. D. McGehee, *Adv. Energy Mater.*, 2012, **2**, 1208.

8 I. McCulloch, M. Heeney, C. Bailey, K. Genevicius, I. MacDonald, M. Shkunov, D. Sparrowe, S. Tierney, R. Wagner, W. Zhang, M. L. Chabinyc, R. J. Kline, M. D. McGehee, M. F. Toney, *Nat. Mater.*, 2006, **5**, 328.

9 M. L. Chabinyc, M. F. Toney, R. J. Kline, I. McCulloch, M. Heeney, *J. Am. Chem. Soc.*, 2007, **129**, 3226.

10 M. Baklar, P. H. Wobkenberg, D. Sparrowe, M. Goncalves, I. McCulloch, M. Heeney, T. Anthopoulos, N. Stingelin, *J. Mater. Chem.*, 2010, **20**, 1927.

11 J. Rivnay, S. C. B. Mannsfeld, C. E. Miller, A. Salleo, M. F. Toney, *Chem. Rev.*, 2012, **112**, 5488.

12 J. E. Parmer, A. C. Mayer, B. E. Hardin, S. R. Scully, M. D. McGehee, M. Heeney, I. McCulloch, *Appl. Phys. Lett.*, 2008, **92**, 113309.

13 A. C. Mayer, M. F. Toney, S. R. Scully, J. Rivnay, C. J. Brabec, M. Scharber, M. Koppe, M. Heeney, I. McCulloch, M. D. McGehee, *Adv. Funct. Mater.*, 2009, **19**, 1173.

14 N. C. Cates, R. Gysel, Z. Beiley, C. E. Miller, M. F. Toney, M. Heeney, I. McCulloch, M. D. McGehee, *Nano Lett.*, 2009, **9**, 4153.

15 N. C. Miller, E. Cho, M. J. N. Junk, R. Gysel, C. Risko, D. Kim, S. Sweetnam, C. E. Miller, L. J. Richter, R. J. Kline, M. Heeney, I. McCulloch, A. Amassian, D. Acevedo-Feliz, C. Knox, M. R. Hansen, D. Dudenko, B. F. Chmelka, M. F. Toney, J. L. Brédas, M. D. McGehee, *Adv. Mater.*, 2012, **24**, 6071.

16 (a) F. C. Jamieson, E. Buchaca- Domingo, T. McCarthy-Ward, M. Heeney, N. Stingelin, J. R. Durrant, *Chem. Sci.*, 2012, **3**, 485; (b) W. L. Rance, A. J. Ferguson, T. McCarthy-Ward, M. Heeney, D. S. Ginley, D. C. Olson, G. Rumbles, N. Kopidakis, *ACS Nano*, 2011, **5**, 5635; (c)T. J. Savenije, W. J.

Grzegorczyk, M. Heeney, S. Tierney, I. McCulloch, L. D. A. Siebbeles, *J. Phy. Chem. C,* 2010, **114**, 15116.

17 (a) J. K. Lee, W. L. Ma, C. J. Brabec, J. Yuen, J. S. Moon, J. Y. Kim, K. Lee, G. C. Bazan, A. J. Heeger, *J. Am. Chem. Soc.*, 2008, **130**, 3619; (b) I. W. Hwang, S. Cho, J. Y. Kim, K. Lee, N. E. Coates, D. Moses, A. J. Heeger, *J. Appl. Phys.*, 2008, **104**, 033706; (c) Y. Gu, C. Wang, T. P. Russell, *Adv. Energy Mater.*, 2012, **2**, 683; (d) N. Shin, L. J. Richter, A. A. Herzing, R. J. Kline, D. M. DeLongchamp, *Adv. Energy Mater.*, 2013, **3**, 938.

18 (a) B. A. Collins, H. Ade, *J. Electron Spectrosc. Relat. Phenom.*, 2012, **185**, 119; (b) A. P. Hitchcock, T. Tyliszezak, I. Koprinarov, H. Stover, W. H. Li, Y. M. Heng, K. Murti, P. Gerroir, J. R. Dutcher, K. Dalnoki-Veress, H. W. Ade, *AIP Conf. Proc.*, 2000, **507**, 231.

19 (a) T. Araki, H. Ade, J. M. Stubbs, D. C. Sundberg, G. E. Mitchell, J. B. Kortright, A. L. D. Kilcoyne, *Appl. Phys. Lett.*, 2006, **89**, 124106; (b) E. Gann, A. T. Young, B. A. Collins, H. Yan, J. Nasiatka, H. A. Padmore, H. Ade, A. Hexemer, C. Wang, *Rev. Sci. Instrum.*, 2012, ***83***, 045110.

20 (a) J. E. Kroeze, T. J. Savenije, M. J. W. Vermeulen, J. M. Warman, *J. Phys. Chem. B*, 2003, **107**, 7696; (b) M. P. De Haas, J. M. Warman, *Chem. Phys.*, 1982, **73**, 35.

21 S. Cook, H. Ohkita, Y. Kim, J. J. Benson-Smith, D. D. C. Bradley, J. R. Durrant, *Chem. Phys. Lett.*, 2007, **445**, 276.

22 O. G. Reid, G. Rumbles, *J. Phys. Chem. Lett.*, 2013, **4**, 2348.

23 D. Veldman, O. Ipek, C. Meskers, J. Sweelssen, M. Koetse, S. Veenstra, J. Kroon, S. v. Bavel, J. Loos, R. Janssen, *J. Am. Chem. Soc.*, 2008, **130**, 7721.

24 I. McCulloch, M. Heeney, C. Bailey, K. Genevicius, I. MacDonald, M. Shkunov, D. Sparrowe, S. Tierney, R. Wagner, W. Zhang, M. Chabinyc, R. Kline, M. McGehee, M. Toney, *Nat. Mater.*, 2006, **5**, 328.

25 A. L. D. Kilcoyne, T. Tyliszczak, W. F. Steele, S. Fakra, P. Hitchcock, K. Franck, E. Anderson, B. Harteneck, E. G. Rightor, G. E. Mitchell, A. P. Hitchcock, L. Yang, T. Warwick, H. Ade, *J. Synchrotron Radiat.*, 2003, **10**, 125.

26 D. Phillips, D. V. O'Connor, *Time-Correlated Single-Photon*, Academic Press, London, 1984.

27 A. Grinvald, I. Z. Steinberg, *Anal Biochem.*, 1974, **59**, 583.

28 (a) G. Dicker, M. P. de Haas, L. D. A. Siebbeles, J. M. Warman, *Phy. Rev. B*, 2004, **70**, 045203; (b) A. J. Ferguson, N. Kopidakis, S. E. Shaheen, G. Rumbles, *J. Phys. Chem. C*, 2008, **112**, 9865.

29 J. Piris, N. Kopidakis, D. C. Olson, S. E. Shaheen, D. S. Ginley, G. Rumbles, *Adv. Funct. Mater.*, 2007, **17**, 3849.

30 T. J. Savenije, M. P. de Haas, J. M. Warman, *Z. Phys. Chem.*, 1999, **212**, 201.

Cite this: DOI: 10.1039/c0xx00000x

www.rsc.org/xxxxxx

COMMUNICATION

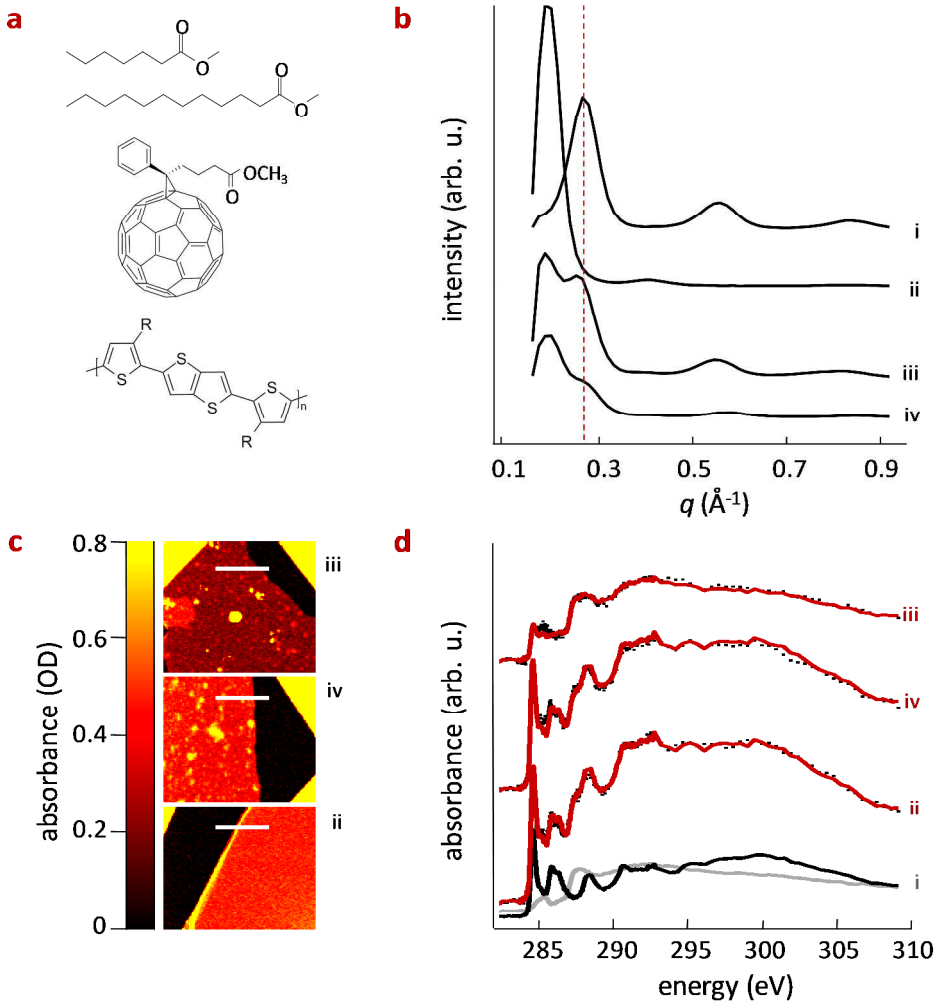

Fig. 1 (a) From top to bottom, chemical structures of Me7, Me12, $PC_{61}BM$ and pBTTT where R=$(CH_2)_{15}CH_3$. (b) Grazing-angle Incidence X-ray diffractograms of neat pBTTT (*i*), pBTTT:$PC_{61}BM$, forming co-crystals (*ii*), pBTTT:Me12:$PC_{61}BM$ (*iii*) and pBTTT:Me7:$PC_{61}BM$ (*iv*). The dashed line indicates the position of the (100) diffraction associated with the lamellar packing distance of the neat polymer at $q \sim 0.28$ Å^{-1}. (c) STXM images (left panels) and absorbance spectra (right panels) of pBTTT:$PC_{61}BM$ (*ii*), pBTTT:Me7:$PC_{61}BM$ (*iv*) and pBTTT:Me12:$PC_{61}BM$ (*iii*) The spectra of neat pBTTT (*i*, grey line) and $PC_{61}BM$ (black line) are included for direct comparison. The absorbance spectra were employed to estimate the composition of each film at the position marked with a white line in the STXM images. We calculate a $PC_{61}BM$ content of approximately 42 wt.% and 43 wt.% for *ii* and *iv,* respectively, indicating the likely presence of an intermixed phase (co-crystal) in such films, while only about 19 wt.% of $PC_{61}BM$ was detected in *iii,* lowering the availability of $PC_{61}BM$ for co-crystal formation.

Cite this: DOI: 10.1039/c0xx00000x

www.rsc.org/xxxxxx

COMMUNICATION

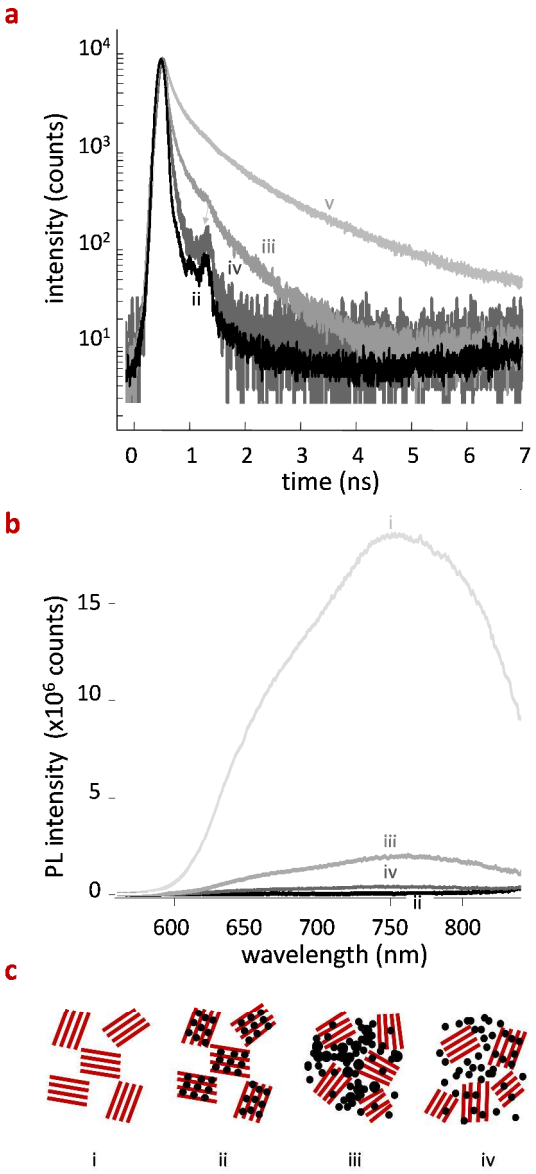

Fig. 2 Photophysical response of films of pBTTT:$PC_{61}BM$ (*ii*), pBTTT:Me12:$PC_{61}BM$ (*iii*), pBTTT:Me7:$PC_{61}BM$ (*iv*) and as reference, pBTTT (*i*) and pBTTT:Me12 (*v*) structures. (a) Photoluminescence decays: faster decays are observed for samples containing a noticeable amount of co-crystal such as *ii* and *iv*; (b) Steady-state photoluminescence (PL) quenching measured for the various systems. The longer alkyl methyl ester (Me12) results in less quenching compared to ternaries comprising Me7. (c) Schematic illustrations of the phase morphologies we deduce from the structural data presented in Figure 1 and results in (a) and (b): pBTTT:$PC_{61}BM$ (*ii*) forms a 1-phase morphology; in pBTTT:Me12:$PC_{61}BM$ ternaries (*iii*), introduction of the additive noticeably expels the fullerene from the polymer leading to a considerable fraction of phase-pure pBTTT and $PC_{61}BM$ regions; while for pBTTT:Me7:$PC_{61}BM$ (*iv*) still a considerable amount of co-crystal is present beside neat polymer and fullerene minority phases. A schematic for the neat polymer (*i*) is also shown.

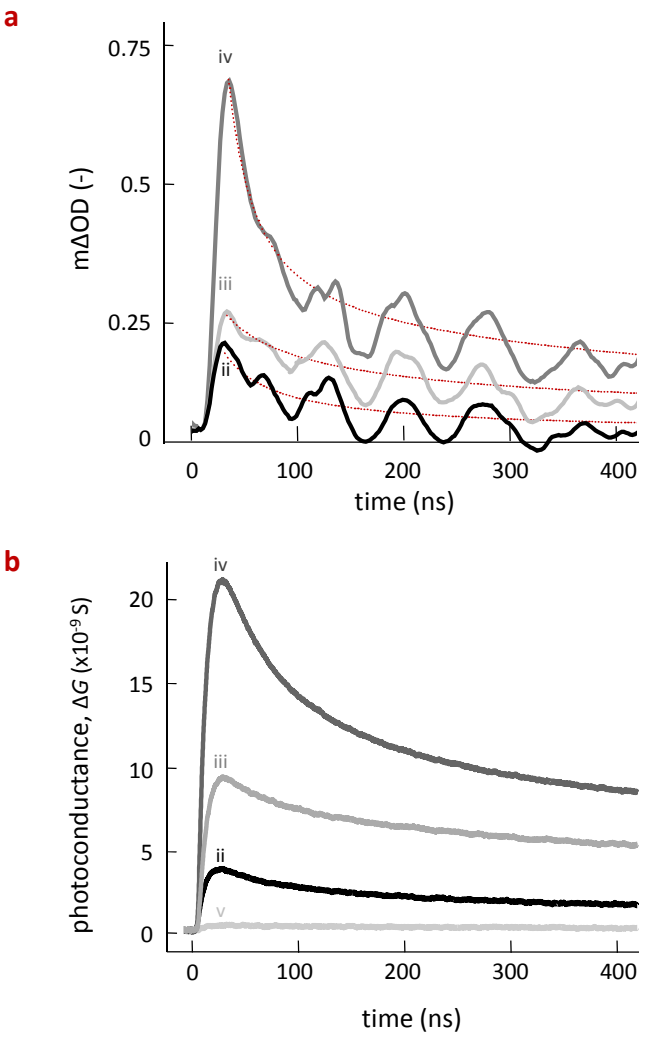

Fig. 3. (a) Transient absorption decay for pBTTT:$PC_{61}BM$ (*ii*), pBTTT:Me12:$PC_{61}BM$ (*iii*), pBTTT:Me7:$PC_{61}BM$ (*iv*) showing the photoinduced absorption of long lived pBTTT polarons following pulsed laser excitation. Highest yield was obtained for ternary comprising the Me7 additive (*iv*) forming a three-phase morphology dominated by the intermixed co-crystal phase. (b) Photoconductance transients, measured by Time-Resolved Microwave Conductivity (TRMC), which follow the same trend in their dynamics and the development of the peak signals as the TAS data: maximum photoconductance is obtained for the ternary system containing Me7 (*iv*). Data for pBTTT:Me12 (*v*) binary is also shown.

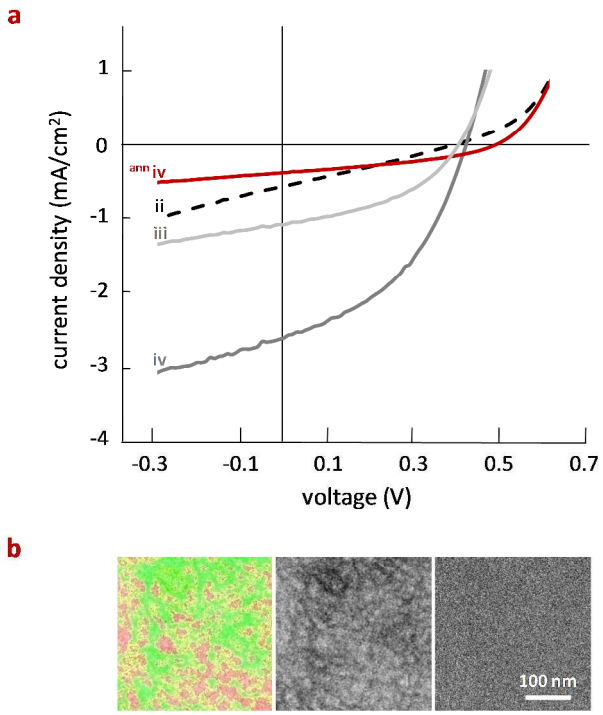

Fig. 4. (a) Current density-voltage (*J-V*) curves for organic photovoltaic (OPV) devices fabricated using active layers comprised of pBTTT:$PC_{61}BM$ (*ii*), pBTTT:Me12:$PC_{61}BM$ (*iii*) and pBTTT:Me7:$PC_{61}BM$ (*iv*). For the 1:1 binary (pBTTT:$PC_{61}BM$) a comparable device performance as reported by Cates *et al.* was measured.[14] The best device performance was obtained for pBTTT:Me7:$PC_{61}BM$ (*iv*), which is comprised of a 3 phases. When annealing this specific ternary (denoted here as ^{ann}*iv*) at 150 °C, which drives fullerene intercalation and, hence, formation of a 1-phase system (see Supplementary Information Figure S4), a *J-V* curve similar to the pBTTT:$PC_{61}BM$ binary is obtained (red line). (b) Electron Spectroscopic Images (ESI) of pBTTT:Me7:$PC_{61}BM$ films before and after annealing at 150 °C (*iv* and ^{ann}*iv*, respectively), illustrating that some phase separation is observed in as-cast structures (left and middle images), while essentially no phase contrast is obtained in annealed samples (right image), indicative of a finely intermixed phase.

Cite this: DOI: 10.1039/c0xx00000x

www.rsc.org/xxxxxx

COMMUNICATION

Table 1. The photophysical and carrier transport properties of pBTTT:$PC_{61}BM$ blends with and without additives

	pBTTT	pBTTT:Me7	pBTTT:Me12	pBTTT:$PC_{61}BM$	pBTTT:Me7:$PC_{61}BM$	pBTTT:Me12:$PC_{61}BM$
$\phi\Sigma\mu$ ($\times10^{-3}$ $cm^2/(Vs)$) [a]	0.38	0.40	0.43	4.99	25.82	11.31
τ_{PL} (ns) [b]	1.08	0.96	0.80	0.054	0.048	0.202
ϕ_{EQ} (%) [c]	--	--	--	95.1	95.0	75.4
mΔOD [d]	--	--	--	0.151	0.693	0.231
$\phi_{CG,TAS}$ (%) [e]	--	--	--	20.7	95.0	36.1
$\phi_{CG,TRMC}$ (%) [f]	2.53	2.68	2.85	33.3	--	--
$\Sigma\mu$ ($\times10^{-3}$ $cm^2/(Vs)$)	15.0 [g]	15.0 [g]	15.0 [g]	15.0 [g]	> 27.2 [h]	15.0 – 31.3 [i]

a] Calculated from the extrapolation of the peak photoconductance to low absorbed photon flux using Equation 3 (Experimental Section). [b] Measured using time-correlated single-photon counting. [c] Calculated from the exciton lifetimes for the corresponding pBTTT:Me7 and pBTTT:Me12 sample with and without $PC_{61}BM$. [d] Amplitude of transient absorption signals measured at ~ 44 ns, probing the polymer cations in all cases. [e] Calculated from the amplitude of the transient absorption signals (mΔOD) of each system relative to the pBTTT:Me7:$PC_{61}BM$, assuming that the charge generation yield ($\phi_{CG,TAS}$) and exciton quenching yield (ϕ_{EQ}) are equivalent for pBTTT:Me7:$PC_{61}BM$—this assumption means that these values represent upper limits estimated using TAS measurements. [f] Calculated from $\phi\Sigma\mu$ assuming that [g] only mobile holes in the polymer contribute to the photoconductance with a high-frequency mobility of 0.015 $cm^2/V.s$.[22] [h] Calculated as a lower limit the for sum of mobilities, assuming that the exciton quenching yield (ϕ_{EQ}) for that sample represents an upper limit for the transient absorption spectroscopy charge generation yield ($\phi_{CG,TAS}$) for the pBTTT:Me7:$PC_{61}BM$ sample. [i] Calculated using the exciton quenching yield (ϕ_{EQ}) and the transient spectroscopy charge generation yield ($\phi_{CG,TAS}$) as upper and lower limits, respectively, for the actual charge generation yield measured by TRMC.